Advances in Radiation Oncology (2024) 9, 101314

advances in radiation oncology

www.advancesradonc.org

Scientific Article

Initial Observation of Contrast Profiles for 2-Dimensional and 3-Dimensional Magnetic Resonance Imaging Sequences in Magnetic Resonance–Guided Radiation Therapy for Locally Advanced Pancreatic Cancer

Gobind S. Gill, MD,* Brady Hunt, PhD, Rongxiao Zhang, PhD, Benjamin B. Williams, PhD, and Bassem I. Zaki, MD

Dartmouth Cancer Center, One Medical Center Drive, Lebanon, New Hampshire

Received 5 April 2023; accepted 3 July 2023

Purpose: In our experience treating locally advanced pancreatic cancer with magnetic resonance–guided radiation therapy (MRgRT), the true-fast imaging with steady-state free precession sequences used to generate both the real-time 2-dimensional (2D) magnetic resonance images (MRI; 2D cine) and the pretreatment high-resolution 3-dimensional (3D) MRI impart differing intensities for relevant structures between the 2 scans. Since these variations can confound target tracking selection, we propose that an understanding of the differing contrast profiles could improve selection of tracking structures.

Methods and Materials: We retrospectively reviewed both 2D cine and 3D MRI images for 20 patients with pancreatic cancer treated with MRgRT. At simulation, an appropriate tracking target was identified and contoured on a single 3-mm sagittal slice of the 3D MRI. This sagittal slice was directly compared with the coregistered 7-mm 2D cine to identify structures with notable discrepancies in signal intensity. The 3D MRI was then explored in additional planes to confirm structure identities. For quantitative verification of the clinically observed differences, the pixel intensity distributions of 2D cine and 3D MRI digital imaging and communications in medicine data sets were statistically compared.

Results: In all patients reviewed, arteries (aorta, celiac, superior mesenteric artery, hepatic artery) appeared mildly hyperintense on both scans. However, veins (portal vein, superior mesenteric vein) appeared hyperintense on 2D cine but isointense on 3D MRI. Biliary structures appeared mildly hyperintense on 2D cine but starkly hyperintense on 3D MRI. The pixel intensity distributions extracted from 2D cine and 3D MRI images were confirmed to differ significantly (2 sample Kolmogorov-Smirnov test; test statistic, 0.40; $P < .001$).

Conclusions: There are significant variations in image intensity between the immediate pretreatment 2D cine compared with the initial planning 3D MRI. Understanding variations of image intensity between the different MRI sequences used in MRgRT is valuable to radiation oncologists and may lead to improved target tracking and optimized treatment delivery.

Sources of support: This work had no specific funding.

Research data are not available at this time.

*Corresponding author: Gobind S. Gill, MD; email: Gobind.S.Gill@hitchcock.org

https://doi.org/10.1016/j.adro.2023.101314

Introduction

Modern therapy for pancreatic cancer

Pancreatic cancer (PC) is a highly lethal malignancy with a 5-year survival rate of 11%.[1] At diagnosis, nearly 50% of patients present with locally advanced PC (LAPC). For PC as a whole, an R0 resection seems to be the greatest positive factor affecting outcomes. Although systemic treatment of PC has improved, surgical resection rates remain low, and patients with borderline resectable or unresectable LAPC still have poor outcomes.

It is hypothesized that neoadjuvant treatment can improve rates of R0 resection, local control, and survival;[2] however, there have been conflicting results regarding the optimal neoadjuvant regimen. A phase 3 trial failed to demonstrate a benefit with the addition of neoadjuvant conventionally fractionated radiation therapy to chemotherapy after induction chemotherapy.[3] However, a propensity-matched retrospective review comparing neoadjuvant stereotactic body radiation therapy (SBRT) to conventionally fractionated radiation therapy demonstrated an improved overall survival with SBRT.[4] Other studies have demonstrated higher biologic effective dose with SBRT as a predictor of improved overall survival.[5] A meta-analysis of over 1000 patients across 19 trials concluded that SBRT did not have superior outcomes compared with conventional RT, but they postulated that dose escalation would likely have a clinical benefit.[6] This echoes the sentiment of other studies regarding the dosimetric feasibility of dose-escalating computed tomography (CT)-based SBRT for LAPC on linear accelerators (linacs).[7] Unfortunately, the success of neoadjuvant CT-based SBRT for LAPC has been limited due to excess dose resulting in toxicity to the organs at risk (OARs) and use of nonablative doses that did not clearly demonstrate improved overall survival for inoperable PC.[8,9]

MR-guided adaptive SBRT

MR-guided radiation therapy (MRgRT) is a novel approach using magnetic resonance imaging (MRI) scans, acquired both before and continuously during treatment to enable soft tissue patient positioning, beam gating based on soft tissue tracking, and online adaptive planning. Stereotactic magnetic resonance-guided adaptive radiation therapy (SMART) uses the unique aspects of MRgRT mentioned previously to push radiation target doses higher while respecting established OAR constraints.

Preliminary data of SMART for LAPC from a single institution demonstrated grade 3 toxicities at only a ~3% rate with a median follow up of 10.3 months.[10] A multicenter phase 2 trial, which recently closed to accrual, implemented SMART in an effort to increase biologic effective dose to 100 Gy using an integrated 0.35T MR-cobalt or MR-linac system (ViewRay Inc, MRIdian, Denver, CO).[11] Details regarding the MR-cobalt and MR-linac technologies and associated workflow have previously been reported.[12,13] The gross tumor volume was defined as the tumor. The clinical target volume (CTV) was defined as gross tumor volume with or without regional lymph nodes, and a 3-mm margin was used for planned target volume construction. The prescription dose was 50.0 Gy in 5 fractions.

Per protocol, before every treatment, a volumetric MRI scan (3-dimensional [3D] MRI) was performed to visualize anatomic changes and predict radiation dose to both target volumes and OARs as per the original plan. When OAR constraints were violated because of anatomic changes, the study required that on-table adaptive planning be performed to ensure OAR constraints were met; optimizing target volume coverage was a secondary objective. The original plan was not delivered if: 1) a gastrointestinal OAR constraint was violated; 2) coverage of the CTV was <85% by the 47.5 Gy isodose line; or 3) there was a favorable shift in CTV and OAR doses in the adaptive plan such that the CTV coverage by the 47.5 Gy isodose line is improved by 10% or more compared with the original plan. On-table plan adaptation, plan evaluation, and adaptive quality assurance occurred while the patient remained in the treatment position. During treatment delivery, sagittal planar MR images (2-dimensional [2D] cine) were continuously acquired during treatment delivery at either 4 or 8 frames per second, and the radiation beam was automatically paused when the tracked pancreatic tumor moved, typically due to respiratory motion, out of a defined gating boundary.

MR sequences

True fast imaging with steady-state free precession is a T1/T2 weighted MRI sequence which uses steady states of magnetizations through gradient reversal echoes and short repetition time between successive excitation pulses, thereby offering high signal-to-noise ratio per unit time.[14] Work has been done for decades to improve these methods and preserve high signal-to-noise in the presence of motion.[15] During MRgRT image acquisition, true fast imaging with steady-state free precession sequences are used for obtaining both the real-time treatment tracking scan, which observes motion on a 2D sagittal slice and the 3D treatment planning scan. However, due to different pulse sequences and levels of magnetization at image acquisition time, which are required to generate the 2D real-time cine and the initial pretreatment 3D setup MRI, there is a large discrepancy in the intensity of relevant anatomic structures. Based on this background, we aimed

at devising a qualitative guide to help establish a rule of thumb for physicians using the MRgRT system.

Methods and Materials

Accessing image sets

With institutional review board approval, digital imaging and communications in medicine files for both 2D cine images and 3D MRI images stored in the treatment planning system were retrospectively accessed for patients with PC (n = 20) treated on the MR-linac. At the time of simulation, an appropriate tracking target was identified and contoured on a single 3-mm sagittal slice of the 3D MRI. At our institution, the default structure selected for tracking is often the visible tumor.

This sagittal slice from the 3D MRI was then directly compared with the coregistered 7-mm 2D cine to identify structures with notable discrepancies in signal intensity paying particular interest to arteries, veins, and biliary structures. The 3D MRI was then explored in additional planes to confirm structure identities. This process is summarized in Fig. 1.

Qualitative description

We qualitatively identified the relative intensity of arteries (specifically the aorta, celiac axis, and superior mesenteric artery [SMA]), veins (portal vein [PV] and superior mesenteric vein [SMV]), and biliary radicles (common bile duct [CBD] and pancreatic duct [PD]).

The relative intensity of each structure was compared between sequences. Any structure that was bright was labeled hyperintense; hyperintensity was subdivided into starkly hyperintense and mildly hyperintense. Any structure that was dark was labeled hypointense. Any structure with similar intensity to surrounding structures or tissues was labeled isointense. All qualitative analyses were performed independently by 2 radiation oncologists and reviewed with a medical physicist and the machine learning research scientist who performed the quantitative analysis.

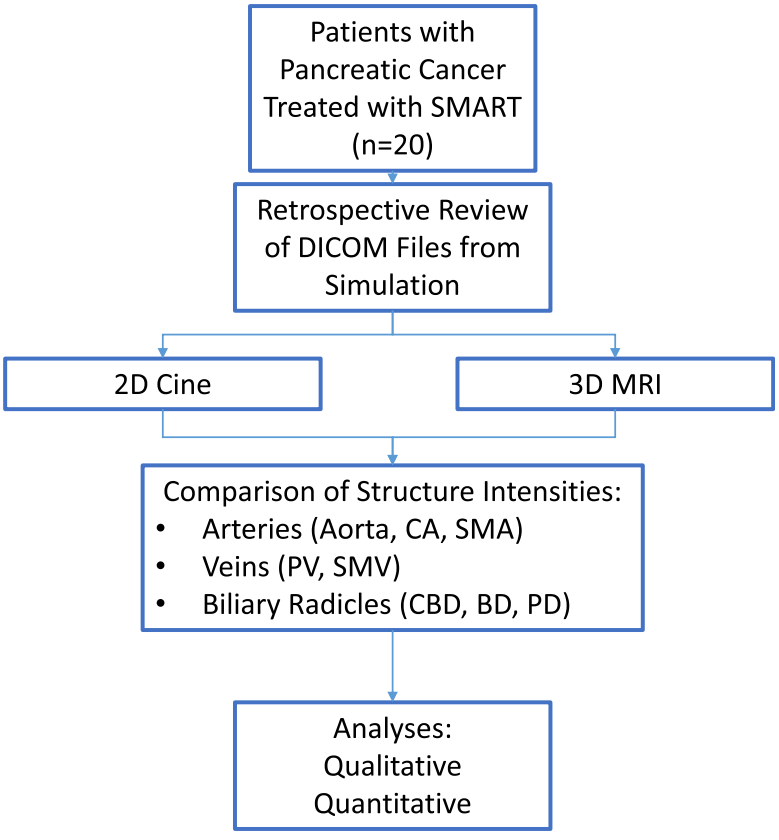

Figure 1 Schema of our methodology for reviewing and comparing the contrast profiles for structures on 2D cine and 3D MRI scans. *Abbreviations:* 2D/3D = two-dimensional/three-dimensional; BD = bile duct; CBD = common bile duct; DICOM = digital imaging and communications in medicine; MRI = magnetic resonance imaging; PD = pancreatic duct; PV = portal vein; SMA = superior mesenteric artery; SMART = stereotactic magnetic resonance-guided adaptive radiation therapy; SMV = superior mesenteric vein.

Quantitative verification

A custom Python script was used to read the raw image data from MRI digital imaging and communications in medicine files using the open source PyDicom module (https://zenodo.org/record/5543955#.Y0nnUXbMLHI). Before intensity distribution comparison, the 3D MRI volume with in-plane resolution of 1.5 × 1.5 mm was resampled to match the in-plane resolution of the cine scan (2.4 × 2.4 mm), and the 2D slice closest to the axial location as the cine scan was extracted from each 3D volume. Additionally, a single frame in the deep breath hold position was sampled for comparison to the 3D scan. Pixel intensities values across all images were concatenated to form the 2 samples: MRI setup scan and MRI cine scan intensities. These samples were then compared using a 2-sample Kolmogorov-Smirnov test available from SciPy (https://docs.scipy.org/doc/scipy-1.7.1/reference/reference/generated/scipy.stats.ks_2samp.html). Additionally, the intensity distributions were visualized using a histogram plot generated using Matplotlib (https://matplotlib.org/stable/api/_as_gen/matplotlib.pyplot.hist.html).

Results

Case 1

Our first example involves a 65-year-old female patient who initially presented with weight loss and jaundice. Workup led to diagnosis of a T4N0M0, stage III (American Joint Committee on Cancer [AJCC] eighth edition) unresectable adenocarcinoma of the pancreatic head. She underwent 7 cycles of neoadjuvant chemotherapy (4 cycles of FOLFIRINOX, switched to 3 cycles of gemcitabine/paclitaxel due to inadequate response). Restaging workup demonstrated a decreased CA-19-9 and a partial response to chemotherapy on MRI. She then underwent preoperative SMART to the pancreatic head tumor in 50 Gy in 5 fractions. She was slated for pancreaticoduodenectomy, which was aborted due to inability to separate the tumor from the common hepatic artery (CHA) or the replaced right hepatic artery originating from the SMA. The replaced right hepatic artery is visualized in Fig. 2.

Figure 2 illustrates the qualitative differences in contrast profiles between the 2D cine (panel A) and the 3D MRI (panel B) observed in her case. In both panels, the tumor is seen contoured in red. Additionally, the yellow contour in panel A represents an expansion boundary used for MRgRT beam gating. Superior to the tumor, in both panels, the confluence of the PD/CBD (light green label) is observed as hyperintense; however, in panel B, it is seen as starkly hyperintense. Immediately superior to the PD/CBD confluence, the PV (blue label) is seen hyperintense on the 2D cine, yet it appears isointense on the 3D MRI. Posterior and anterior to the PV, respectively, the right and left branches of the hepatic artery (red) are visualized with similar intensity on both scans.

Case 2

Our next case is a 72-year-old man who initially presented with dyspepsia, abdominal pain, and weight loss. Workup led to diagnosis of a T4N0M0, stage III (AJCC eighth edition) borderline resectable ~3-cm adenocarcinoma of the pancreatic head with involvement of the SMA. He underwent 8 cycles of neoadjuvant mFOLFIRINOX. Restaging workup demonstrated good response via

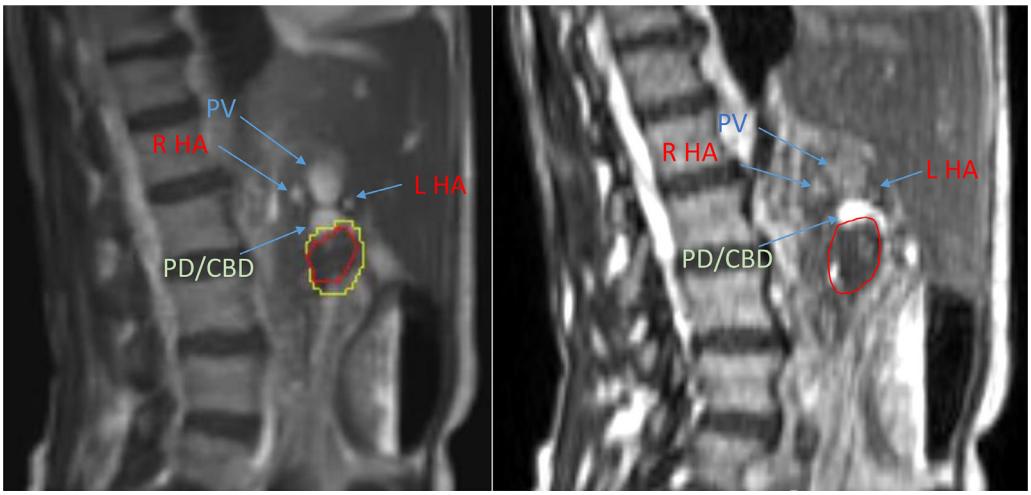

Figure 2 Case 1 images. Comparison of (A) sagittal slices of the 2D cine to the corresponding (B) 3D MRI for case 1. *Abbreviations:* 2D/3D = two-dimensional/three-dimensional; CBD = common bile duct; HA = hepatic artery; L = left; MRI = magnetic resonance imaging; PD = pancreatic duct; PV = portal vein; R = right.

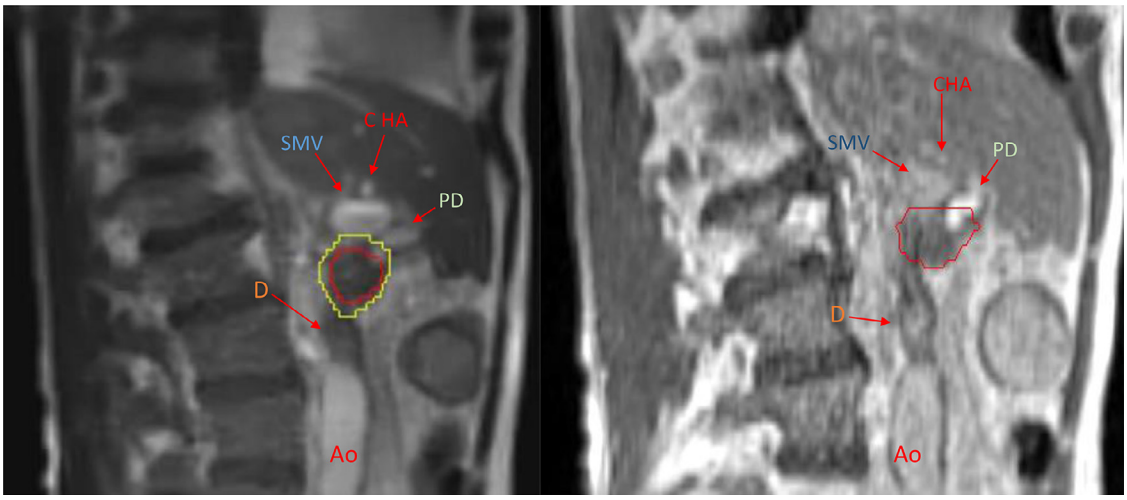

Figure 3 Case 2 images. Comparison of (A) sagittal slices of the 2D cine to the corresponding (B) 3D MRI for case 2. *Abbreviations:* 2D/3D = two-dimensional/three-dimensional; Ao = aorta; CHA = common hepatic artery; D = duodenum; MRI = magnetic resonance imaging; PD = pancreatic duct; SMV = superior mesenteric vein.

CA-19-9 and CT scan of the abdomen. He subsequently completed preoperative SMART to the pancreatic head tumor in 50 Gy in 5 fractions. He successfully underwent pancreaticoduodenectomy with pathology demonstrating residual ductal adenocarcinoma of the pancreatic head and metastases in 3 of 12 lymph nodes examined, ypT2N1.

His anatomy can be visualized in Fig. 3. In both panels, the tumor is seen contoured in red. As in case 1, the yellow contour in panel A represents an expansion boundary used for MRgRT beam gating. Superior to the tumor, in both panels, the SMV (blue label) is observed as hyperintense; however, in panel B, it is seen as isointense. Immediately anterior to the SMV, the PD (light green label) is seen as hyperintense on the 2D cine, yet it appears starkly hyperintense on the 3D MRI. Superior to the SMV, the CHA (red) is visualized to be hyperintense in both scans. Inferior to the tumor, the duodenum (orange) can be visualized in both scans, and inferior to the duodenum, the aorta (red) can be visualized as hyperintense in both scans.

Case 3

Our final case is a 69-year-old man who initially presented with abdominal pain and jaundice. Workup led to diagnosis of a T2N0M0, stage II (AJCC eighth edition) borderline resectable 3.5-cm adenocarcinoma of the pancreatic head. He underwent biliary stenting followed by 7 cycles of neoadjuvant mFOLFIRINOX. Restaging workup demonstrated good response via CA-19-9 and CT of the abdomen. He subsequently completed preoperative SMART to the pancreatic head tumor in 50 Gy in 5 fractions. He underwent pancreaticoduodenectomy successfully with pathology demonstrating residual ductal adenocarcinoma of the pancreatic head, ypT2N0.

His anatomy can be visualized in Fig. 4. In both panels, the tumor is seen contoured in red. As in our prior cases, the yellow contour in panel A represents an expansion boundary used for MRgRT beam gating. Superior to the tumor, in both panels, the CBD (light green label) is observed as hyperintense; however, in panel B, it is seen as starkly hyperintense. Immediately superior and posterior to the CBD, the PV (blue label) is seen hyperintense on the 2D cine, yet it appears isointense on the 3D MRI. Superior to the PV, the CHA (red) is visualized to be mildly hyperintense in both scans. Anterior to the tumor, the duodenum (orange) is visualized in both scans. Posterior to the tumor, the inferior vena cava (blue) is visualized as hyperintense on the 2D cine yet isointense on the 3D MRI.

Qualitative findings

In all 20 patients reviewed, arteries (aorta, celiac, SMA, HA) typically appeared with mild hyperintensity resulting in similar contrast profiles in both scans. However, veins (PV, SMV) appeared consistently hyperintense on 2D cine and consistently isointense on 3D MRI. Biliary structures (CBD, PD) appeared consistently hyperintense on both scans, only mildly hyperintense on 2D cine, but starkly hyperintense on 3D MRI. These findings are summarized in Table 1.

Quantitative verification

The pixel intensity distributions extracted from 2D cine and 3D MRI images were confirmed to differ significantly (2-sample Kolmogorov-Smirnov test; test statistic, 0.40; $P < .001$) (Fig. 5).

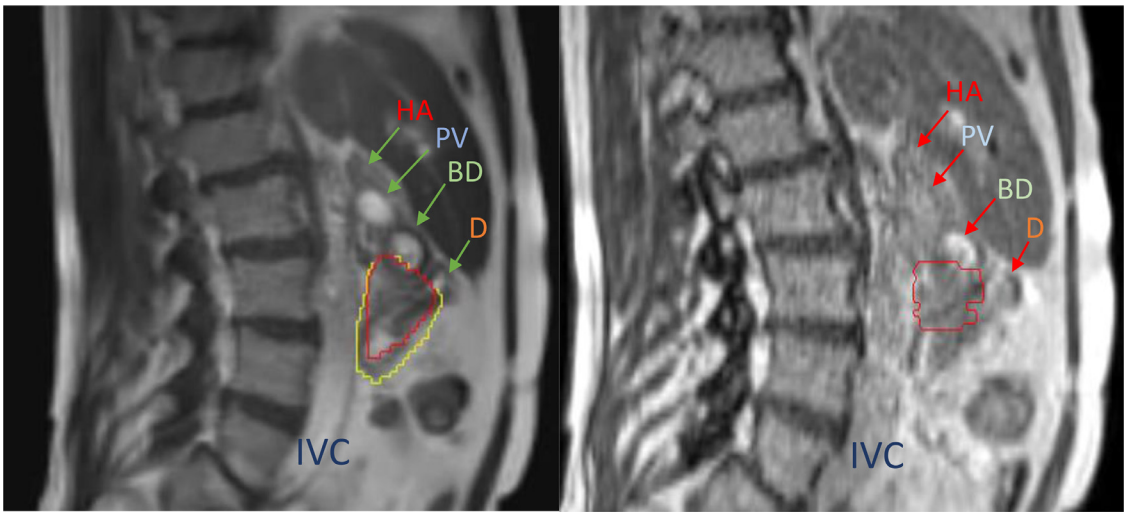

Figure 4 Case 3 images. Comparison of (A) sagittal slices of the 2D cine to the corresponding (B) 3D MRI for case 3. *Abbreviations:* 2D/3D = two-dimensional/three-dimensional; BD = bile duct; D = duodenum; HA = hepatic artery; IVC = inferior vena cava; PV = portal vein.

Table 1 Qualitative results of clinically observed intensity of arteries, veins, and biliary radicles on both 2D cine and 3D MRI sequences

Structure reviewed	2D cine	3D MRI
Arteries (aorta, celiac, SMA, HA)	Mildly hyperintense	Mildly hyperintense
Veins (PV, SMV)	Hyperintense	Isointense
Biliary radicles (CBD, PD)	Mildly hyperintense	Starkly hyperintense

Abbreviations: 2D/3D = 2-dimensional/3-dimensional; CBD = common bile duct; HA = hepatic artery; MRI = magnetic resonance imaging; PD = pancreatic duct; PV = portal vein; SMA = superior mesenteric artery; SMV = superior mesenteric vein.

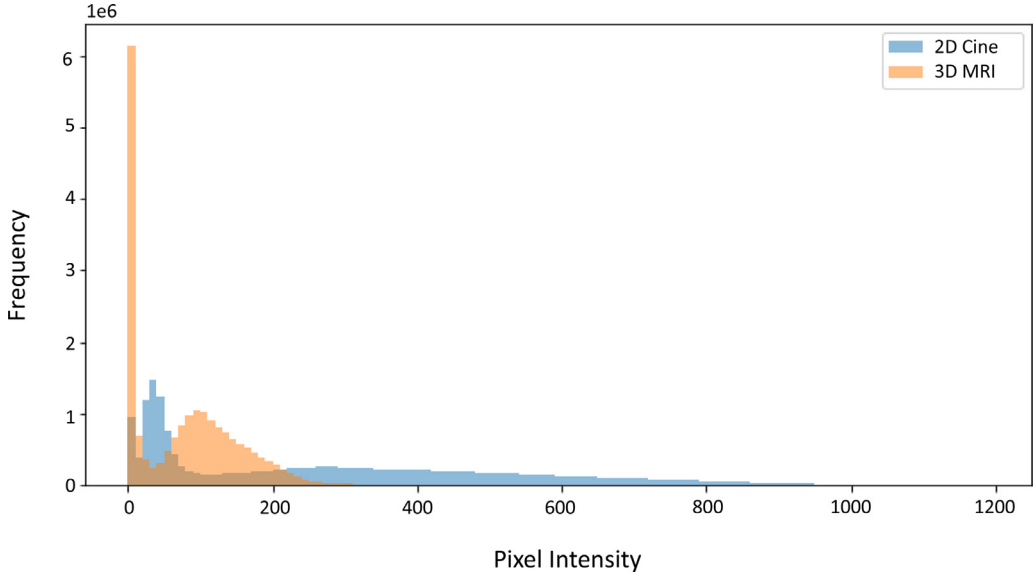

Figure 5 Pixel intensity histogram. Comparison of pixel intensity distributions for 2D cine and 3D MRI images. *Abbreviations:* 2D/3D = two-dimensional/three-dimensional; MRI = magnetic resonance imaging.

Discussion

Our findings qualitatively confirm our hypothesis that arteries, veins, and biliary radicles do appear with different intensities on 2D cine versus the 3D MRI during SMART. Additionally, Fig. 5 demonstrates the disparity in pixel intensity between the 2 data sets. We hypothesize that this difference in intensity may have to do with the biophysical characteristics of the fluid content including velocity of fluid and/or oxygen content of the conduits, particularly in arteries.

Understanding these significant variations of image intensity between the immediate pretreatment 2D cine and the initial treatment planning 3D MRI can guide radiation oncologists in choosing optimal tracking targets. For example, if a tracking structure is selected due to its relative intensity to the background based on the 3D MRI, this may, in fact, not be consistent with the relative intensity to background on 2D cine and lead to tracking target failure, which could lead to improper/inefficient gating or the need for contouring an alternative tracking target. Any of these scenarios could potentially cause confusion or uncertainty of the treatment team at the time of radiation delivery. Furthermore, all of these situations could lead to increased time for delivery and increased time on table in an enclosed MR-linac.

A limitation of this study is the small number of patient images that were reviewed. To enhance comparability between images obtained for different patients, we limited our review to images for patients with a diagnosis of PC who were treated on one 0.35T MR-linac in this single institution study. By including other diagnoses spanning different anatomic sites and expanding the study to include other institutions which may have a 1.5T MR-linac, we can sizably increase the patient cohort, improve generalizability of the study, and compare/contrast our findings on the 0.35T MR-linac with the 1.5T MR-linac.

The ViewRay system is slated to upgrade to 3D target tracking. Although this would not affect the contrast profiles of the 2D cine or the 3D MRI, it would allow for more information to confirm anatomic identity of structures due to the ability to track with a 3D cine. Lastly, our group is working on a generative deep learning approach to match the contrast profiles between the 2D cine and the 3D MRI scans. In addition, we are exploring alternative deep learning–based tracking algorithms which could improve the ViewRay user experience.

Conclusion

Understanding variations of image intensity between the different MRI sequences used in SMART, or MRgRT at large, is valuable to radiation oncologists and may lead to improved target tracking.

Disclosures

The authors declare that they have no known competing financial interests or personal relationships that could have appeared to influence the work reported in this paper.

Acknowledgments

The authors thank Charles R. Thomas Jr, MD.

References

1. Siegel RL, Miller KD, Fuchs HE, Jemal A. Cancer statistics, 2022. *CA Cancer J Clin*. 2022;72:7-33.
2. Versteijne E, van Dam JL, Suker M, et al. Neoadjuvant chemoradiotherapy versus upfront surgery for resectable and borderline resectable pancreatic cancer: Long-term results of the Dutch randomized PREOPANC trial. *J Clin Oncol*. 2022;40:1220-1230.
3. Hammel P, Huguet F, van Laethem JL, et al. Effect of chemoradiotherapy versus chemotherapy on survival in patients with locally advanced pancreatic cancer controlled after 4 months of gemcitabine with or without erlotinib: The LAP07 randomized clinical trial. *JAMA*. 2016;315:1844-1853.
4. Zhong J, Patel K, Switchenko J, et al. Outcomes for patients with locally advanced pancreatic adenocarcinoma treated with stereotactic body radiation therapy versus conventionally fractionated radiation: SBRT versus conventional RT in LAPC. *Cancer*. 2017;123:3486-3493.
5. Rudra S, Jiang N, Rosenberg SA, et al. Using adaptive magnetic resonance image-guided radiation therapy for treatment of inoperable pancreatic cancer. *Cancer Med*. 2019;8:2123-2132.
6. Petrelli F, Comito T, Ghidini A, Torri V, Scorsetti M, Barni S. Stereotactic body radiation therapy for locally advanced pancreatic cancer: A systematic review and pooled analysis of 19 trials. *Int J Radiat Oncol Biol Phys*. 2017;97:313-322.
7. Mazzarotto R, Simoni N, Guariglia S, et al. Dosimetric feasibility study of dose escalated stereotactic body radiation therapy (SBRT) in locally advanced pancreatic cancer (LAPC) patients: It is time to raise the bar. *Front Oncol*. 2020;10: 600940.
8. Katz MHG, Shi Q, Meyers J, et al. Efficacy of preoperative mFOLFIRINOX versus mFOLFIRINOX plus hypofractionated radiotherapy for borderline resectable adenocarcinoma of the pancreas: The A021501 phase 2 randomized clinical trial. *JAMA Oncol*. 2022;8:1263-1270.
9. Janssen QP, van Dam JL, Prakash LR, et al. Neoadjuvant radiotherapy after (m)FOLFIRINOX for borderline resectable pancreatic adenocarcinoma: A TAPS Consortium study. *J Natl Compr Canc Netw*. 2022;20(7):783-791.e1.
10. Chuong MD, Bryant J, Mittauer KE, et al. Ablative 5-fraction stereotactic magnetic resonance–guided radiation therapy with on-table adaptive replanning and elective nodal irradiation for inoperable pancreas cancer. *Pract Radiat Oncol*. 2021;11:134-147.
11. Parikh PJ, Lee P, Low D, et al. Stereotactic MR-guided on-table adaptive radiation therapy (SMART) for patients with borderline or

locally advanced pancreatic cancer: Primary endpoint outcomes of a prospective phase II multi-center international trial. *Int J Radiat Oncol Biol Phys*. 2022;114:1062-1063.

12. Herman JM, Chang DT, Goodman KA, et al. Phase 2 multi-institutional trial evaluating gemcitabine and stereotactic body radiotherapy for patients with locally advanced unresectable pancreatic adenocarcinoma. *Cancer*. 2015;121:1128-1137.
13. Reyngold M, Parikh P, Crane CH. Ablative radiation therapy for locally advanced pancreatic cancer: Techniques and results. *Radiat Oncol*. 2019;14:95.
14. Zur Y, Bosak E, Kaplan N. A new diffusion SSFP imaging technique. *Magn Reson Med*. 1997;37:716-722.
15. Zur Y, Wood ML, Neuringer LJ. Motion-insensitive, steady-state free precession imaging. *Magn Reson Med*. 1990;16:444-459.